Arabian Journal of Chemistry (2023) **16**, 104836

King Saud University

Arabian Journal of Chemistry

www.ksu.edu.sa
www.sciencedirect.com

ORIGINAL ARTICLE

Simultaneous removal and conversion of silver ions from wastewater into antibacterial material through selective chemical precipitation

Da Li [a], Xueyun Zhang [b], Xiaozhong Liang [a], Wen Liu [b], Kunpeng Guo [a,*], Zheng Zhang [a], Sijing Wang [a], Yifan Xing [a], Zhijun Li [a], Jie Li [a,*], Hua Wang [a]

[a] *Ministry of Education Key Laboratory of Interface Science and Engineering in Advanced Materials, Research Center of Advanced Materials Science and Technology, Taiyuan University of Technology, Taiyuan 030024, China*
[b] *School of Basic Medical Sciences, Shanxi Medical University, Taiyuan 030001, China*

Received 15 December 2022; accepted 19 March 2023
Available online 23 March 2023

KEYWORDS

Silver recovery;
Wastewater;
Selective chemical precipitation;
Antibacterial material;
Planar precipitant

Abstract High doses of silver compounds in water have been found to be extremely toxic to the cells of plants and animals. Removal then reutilization of silver ions as antibacterial materials in one step from wastewater is an urgent but challenging issue from the views of environment and economy. In this research, we reported a planar benzothiazole Schiff base derivative **BTS1** that can selectively precipitate silver ions from wastewater over other metal ions through chemical precipitation. The precipitation reaction showed promising activity in the pH range of 6 to11, realizing a high silver ions precipitation ratio of 95.4%, and low LOD of 0.059 mg/L. More importantly, the filtrated precipitate **BTS1-Ag** can be directly used as an antibacterial material. The test papers coated with **BTS1-Ag** exhibited antibacterial activity against both gram-positive and gram-negative bacteria. This research provides a promising strategy for simultaneous removal and conversion of silver ions from wastewater into functional materials.

1. Introduction

The removal and recovery of precious metals from wastewater have drawn great attention due to the low abundance of these raw metal resources and risk in ecology. (Ling et al., 2018; Qian et al., 2020; Yang et al., 2020; Wang et al., 2023) As one of the most important and useful precious metals, silver possesses wide application in electroplating, photography, batteries, electronics, (Ibrahim et al., 2022) catalysis, (Xue et al., 2020) biomedical, (Chernousova and Epple, 2013) photonics and dental materials due to its unique photosensitivity and bioactivity. (Wang et al., 2020) In this context, a large amount of silver ions-rich industrial wastewater has been discharged into the

* Corresponding authors.
E-mail addresses: guokunpeng@tyut.edu.cn (K. Guo), lijie01@tyut.edu.cn (J. Li).

Peer review under responsibility of King Saud University.

Production and hosting by Elsevier

https://doi.org/10.1016/j.arabjc.2023.104836

natural environment. Recently, growing concerns have been raised on its accumulated toxicity on the cells of plants and animals. (Ratte, 1999; Ahmad et al., 2019; Xie et al., 2022) Besides, direct discharge of silver ions-rich wastewater is also a waste of resources in consideration of the limited stock of precious metals on earth. (Akcil et al., 2015; Sverdrup et al., 2014; Wang et al., 2020) In 2011, the US Water Environment Research Foundation (WERF) reported that treating wastewater 10 million gallon per day may have the potential to recover $8849-$3,904,664 worth of silver worth per year. (Ho and Babel, 2021) Therefore, the highly selective recovery of silver ions from the wastewater containing multi-metal ions for further utilization demonstrates extreme importance from the view of environment and economy. To date, plenty of methods and techniques including membrane filtration, electrolysis, chemical precipitation, cementation, adsorption, ion exchange, electrowinning, solvent extraction and bioelectrochemical system have been developed to recover silver from wastewater. (Wang and Ren, 2014; Xu et al., 2018; Wen et al., 2013) The chemical precipitation attracts wide attentions on account of its eco-friendship, low cost, and easy operation. (Fu et al., 2007; Ying and Fang, 2006; Chen et al., 2018; Quiton et al., 2022).

As the core of chemical precipitation, various inorganic sulfide precipitants have been adopted for silver recovery, such as Na_2S, K_2S, NaHS, NH_4HS and $Na_2S_2O_3/Na_2S_2O_4$ system. In these cases, strict dosage control is needed to avoid possible accidental escape of the toxic hydrogen sulfide. Additionally, the poor selectivity also goes against the exclusive precipitation of silver ions over other metal ions, such as Ca^{2+}, Cu^{2+} and Pb^{2+}. (Bas et al., 2012; Yazici et al., 2017) More importantly, the separated silver sulfide requires further refining process to obtain purified silver or combining with other materials to acquire new functions, which undoubtedly consumes additional energy and resource. (Ho and Babel, 2021) An ideal technology for the treatment of wastewater containing precious metal ions should be able to achieve two goals simultaneously: targeted precious metal ions removal and conversion into useful materials directly. (Ling et al., 2018, W.X. Zhang, 2018) Recently, the prevalence of Covid-19 has forced researchers spanning the globe to focus on the safe and effective antibacterial agents. In this context, silver nanoparticles and silver (I) (Ag^+) complexes with antibacterial activities have received rising attention. (Hamouda et al., 2021; Allawadhi et al., 2021; Morozova et al., 2022; Law et al., 2022; Teirumnieks et al., 2020; Abbas et al., 2022) Thereafter, it is of great significance to design novel precipitants with high specificity and efficiency for selective conversion of silver ions from wastewater into antibacterial materials.

Schiff bases have proven to be effective probes for metal ions through ligand–metal coordination. (Khan et al., 2021) Although some Schiff bases synthesized by heterocyclic structure containing nitrogen and sulphur showed biological activity after complexing with Ag^+ ions, (Adeleke et al., 2021; Mary Jenisha Barnabas et al., 2021) they were rarely employed in the direct conversion of Ag^+ ions from wastewater into antibacterial materials. This is due to the challenge of specific complexation with Ag^+ ions and formation of precipitated antibacterial material simultaneously.

Herein, we reported a planar benzothiazole Schiff base derivative **BTS1** for one-step converting Ag^+ ions from wastewater into antibacterial material via highly selective chemical precipitation (Fig. 1a). In comparison with twisted molecules, the molecule adopting planar structure is aimed to reduce the solubility, and thus is beneficial to enhance precipitating efficiency. Benzothiazole is introduced for its inherent conjugate rigid plane structure and as building block for antibacterial materials. (Zeng et al., 2019; Yan et al., 2020) Besides, the lone pair of electrons on the nitrogen atom of the thiazole ring would enhance the affinity with Ag^+ ions. **BTS1** was synthesized via one-pot condensation of 4-(thiophen-2-yl)benzaldehyde (**1-CHO**) and 2-hydrazinobenzothiazole (**HBT**) in a high yield up to 82% (Fig. 1b). To demonstrate that the planar molecular structure is superior in precipitation, two control benzothiazole Schiff base derivatives **BTS2** and **BTS3** with decreased planarity sequentially were synthesized by replacing **1-CHO** with [2,2′-bithiophene]-5-carbaldehyde (**2-CHO**) and 4-(diphenylamino)benzaldehyde (**3-CHO**), respectively. The precipitation efficiency was decreased from **BTS1** to **BTS2**, and no precipitation was observed in the case of highly twisted **BTS3**. Remarkably, the precipitate **BTS1-Ag** exhibited antimicrobial activity against both gram-positive (*S. aureus*) and gram-negative (*E. coli* and *P. aeruginosa*) bacteria. This work shows the highly potential application of Schiff bases in converting precious metals from wastewater into useful materials.

2. Results and discussion

To understand the configurations of the Schiff bases, single crystals of **BTS1–3** were cultivated from the binary mixture of THF/methanol (v/v, 2/1) at 25 °C (crystallographic data in detail were provided in Tables S1–S3). As shown in Fig. 2a, **BTS1** appeared in an approximately planar configuration from side view with the dihedral angles between the phenyl ring and the adjacent benzothiazolyl and thienyl groups of 3.6° and 3.3°, respectively. **BTS2** exhibited a slightly twisted configuration with the dihedral angles increased to 7.8° and 5.0°, respectively (Fig. 2b). For **BTS3**, the triphenylamine moiety presented highly twisted configuration and the dihedral angle between the phenyl ring and benzothiazolyl unit was up to 22.3°, as shown in Fig. 2c. These results indicated that their solubilities would increase from **BTS1** to **BTS3** due to the increased spatial configuration of the molecules. Besides, three types of intermolecular interactions including S2…S2 (3.514 Å), N1…N2-H (2.946 Å) and N1…H-N2 (2.142 Å) were detected between **BTS1** molecules (Fig. 2d). Assisted by such interactions, planar **BTS1** molecules formed interlaced herringbone patterns (Fig. 2g). More types of intermolecular interactions between **BTS2** molecules and between **BTS3** molecules were found (Fig. 2e and f). These interactions caused **BTS2** and **BTS3** molecules to pack more loosely in face-to-face parallel patterns (Fig. 2h and i). Both in terms of molecular configuration and packing mode, **BTS1** seemed preferable to form precipitates.

Forming precipitates with Ag^+ ions in solution via chemical complexation is the first key issue for **BTS1** to recycle Ag^+ ions effectively from wastewater. So, we studied the precipitation behaviours between **BTS1** (25 μM) and various metal ions (10 mM) in a mixture of H_2O/acetone (v/v, 99/1), respectively. As shown in Fig. 3, before adding metal ions, **BTS1** exhibited two absorption bands centered at 311 nm ($\varepsilon = 2.36 \times 10^4\ M^{-1}\ cm^{-1}$) and 363 nm ($\varepsilon = 1.05 \times 10^5\ M^{-1}\ cm^{-1}$), which were ascribed to π-π* transition of the aromatic rings and n-π* transition related to molecular orbitals of C = N group and thiazole ring, respectively. Remarkably, after adding Ag^+ ions, the absorption intensity at 363 nm dramatically decreased about 86.4 % (Fig. S1a). In this process, a yellow flocculent precipitate emerged rapidly, and the precipitation process completed within seconds (Video S1). However, the absorption peaks remained almost the same after the addition of other metal ions, implying that no complex reaction occurred, or soluble complexes were formed. The results suggest that **BTS1** can selectively precipitate Ag^+ ions in approximate aqueous solution. To investigate the influence of the molecular planarity on the precipitation efficiency, **BTS2** and **BTS3** were also tested in the same condition. As shown in Fig. S1b and c, partial decline (51.5%) and nearly no decline (1.3%) of absorbance were found after adding Ag^+ ions into the solution of **BTS2** and **BTS3**, respectively. Therefore, from the view of molecular

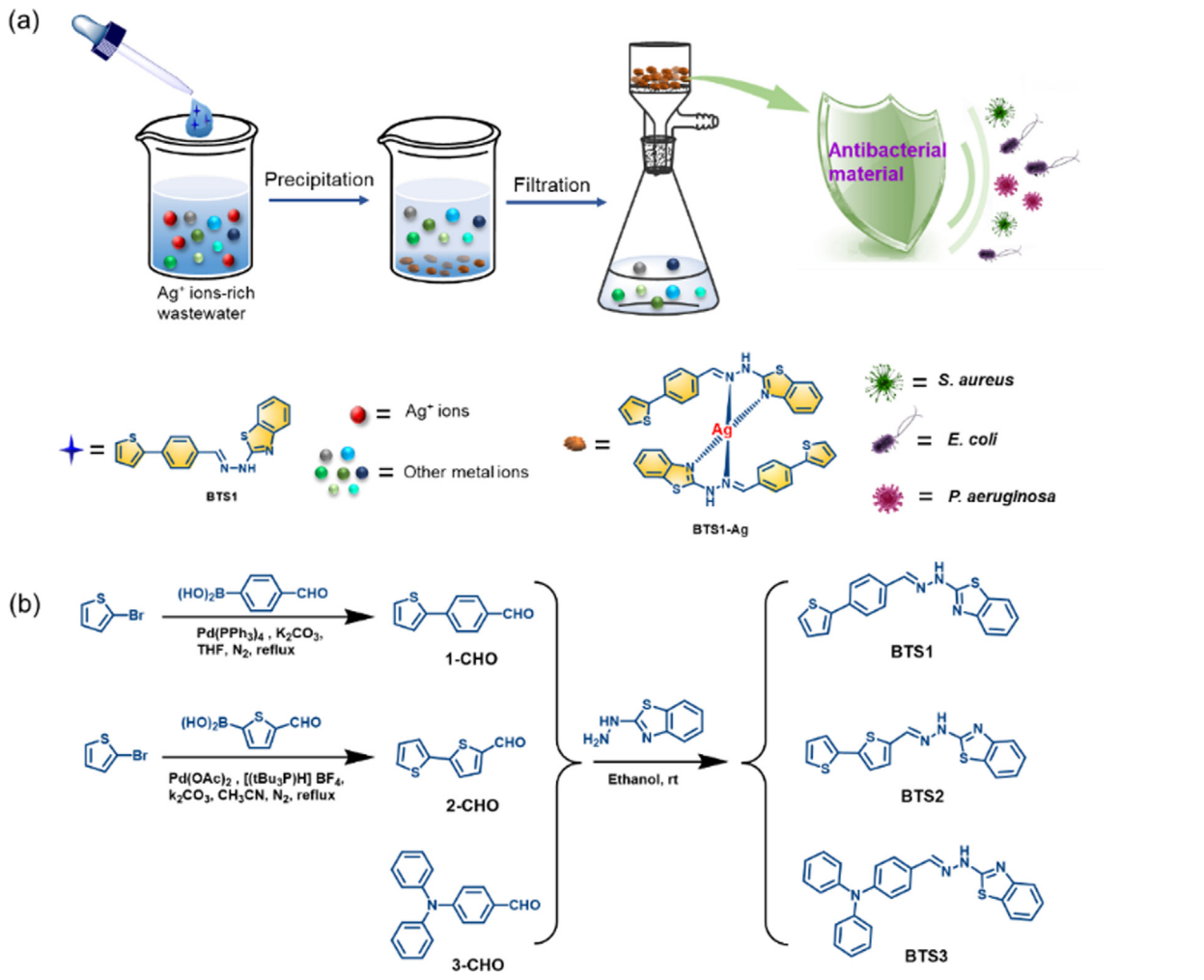

Fig. 1 (a) Graphical illustration of recovery and conversion process of Ag^+ ions from wastewater. (b) The synthetic routes of compound **BTS1-3.**

configuration, planar structure (**BTS1**) benefitted to precipitate Ag^+ ions in comparison with nonplanar counterparts (**BTS2** and **BTS3**), which confirmed the feasibility of the proposed molecular design strategy.

The morphology of the yellow precipitates was investigated by scanning electron microscope (SEM) measurement. As shown in Fig. S2a and 2b, **BTS1-Ag** exhibited aggregated nanosheets morphology, indicating the **BTS1-Ag** molecules are tending to form aggregates then precipitate from water. The chemical composition and structure of the precipitate were firstly analysed by elemental mapping and X-ray Photoelectron Spectroscopy (XPS). Elemental mapping analyses indicated C, S and Ag elements are uniformly distributed in the precipitate **BTS1-Ag** (Figure S2c, 2d and 2e). Additionally, the wide-scan XPS spectra indicated that only the yellow precipitate contained Ag3d peak in addition to C1s, S2p, and N1s peaks compared with pure **BTS1**, which verified the presence of silver element in the precipitate (Fig. 4a). Furthermore, the peaks located at 367.7 and 373.7 eV can be assigned to $Ag3d_{5/2}$ and $Ag3d_{3/2}$ (Fig. 4b), which demonstrated that silver existed in the form of Ag(I). (Zhao et al., 2020) Thus, it was suggested that a chemical complexation reaction existed between **BTS1** and Ag^+ ion, which yielded a poorly soluble Ag-complex (named as **BTS1-Ag**) and therefore was responsible for the formation of the precipitate and the disappearance of the absorption peaks.

The coordinate mode of **BTS1** with Ag^+ ions in the complex **BTS1-Ag** was further analysed. As shown in Fig. 5a, the binding energy peaks at 164.0 and 165.3 eV signalled the existence of $S2p_{3/2}$ and $S2p_{1/2}$ orbitals, respectively, which confirmed the confinement of S to C-S bond. (Li et al., 2021) Meanwhile, there were no evident differences in the characteristic peaks of S2p for **BTS1** and **BTS1-Ag**, indicating the S atom has not taken part in complexation of Ag^+ ions. Notably, the N1s core-level spectrum changed obviously after complexing with Ag^+ ions. The N1s core-level spectrum of **BTS1** revealed the existence of three components at the binding energy of 398.25, 399.99 and 401.40 eV, attributable to –NH- nitrogen atom, thiazole nitrogen atom and the imine nitrogen atom, respectively (Fig. 5b). However, after complexing with Ag^+ ions, only two components could be detected at the binding energy of 399.22 and 400.03 eV, which can be assigned to the nitrogen atoms of –NH- and N-Ag, respectively (Fig. 5c). (Qian et al., 2020) Therefore, in comparison with **BTS1**, the disappearance of peaks at 398.25 and 399.99 eV demonstrated the coordination of the imine nitrogen atom

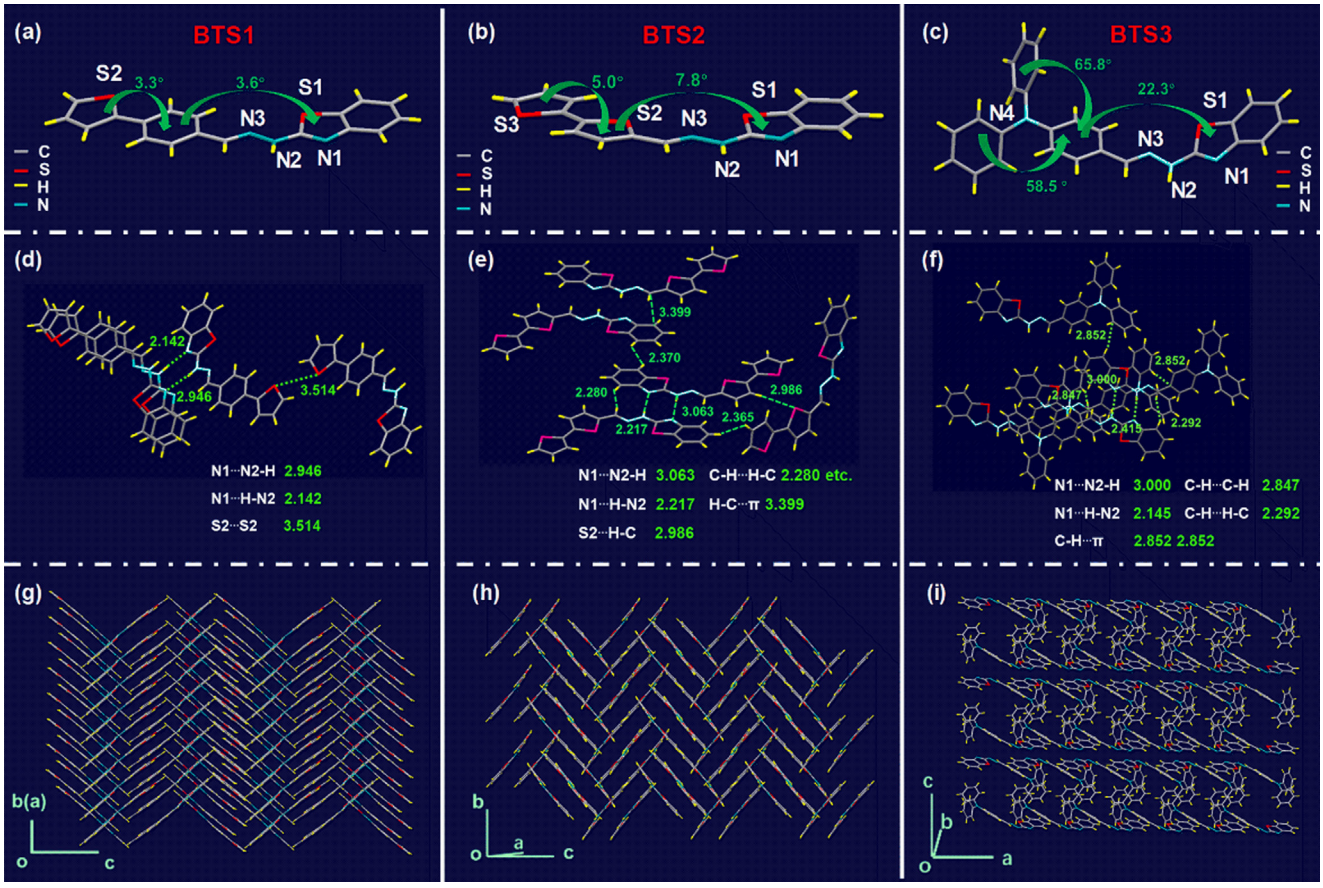

Fig. 2 Molecular structures of (a) **BTS1**, (b) **BTS2**, and (c) **BTS3**. Non-covalent interactions of (d) **BTS1**, (e) **BTS2**, and (f) **BTS3**. Molecular packing of (g) **BTS**1, (h) **BTS2**, and (i) **BTS3**.

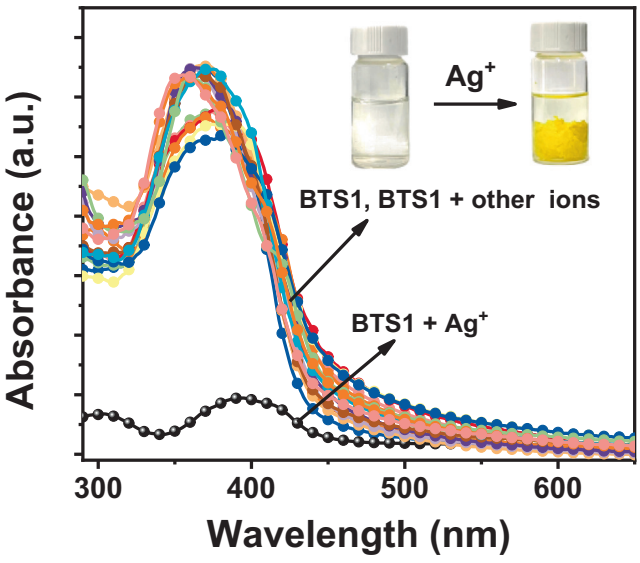

Fig. 3 UV–vis absorption spectra of **BTS1** (25 μM) upon addition of metal ions (10 mM) in H_2O/acetone (v/v, 99/1) (Inset: Changes of **BTS1** solution before and after adding Ag^+ ions under daylight).

and thiazole nitrogen atom with Ag^+ ions in **BTS1-Ag**. The FT-IR spectra of **BTS1** and **BTS1-Ag** further verified the binding sites of Ag^+ ions with **BTS1**. As shown in Fig. 5d, compared with the FT-IR spectra of **BTS1**, only the -C = N- absorption of imine and thiazole was weakened and shifted from 1612 cm^{-1} to 1587 cm^{-1} and 1562 cm^{-1} to 1560 cm^{-1}, respectively. Subsequent experiments were conducted to ascertain the complexation ratio of **BTS1** with Ag^+ ions. A Job's plot obtained from absorption data showed 2:1 stoichiometric complexation between **BTS1** and Ag^+ ions (Fig. 5e). The 2:1 binding stoichiometry was further confirmed by electrospray ionization (ESI) mass spectra. A peak of $[2\mathbf{BTS1} + Ag]^+$ at m/z 778.004 and a peak of $[2\mathbf{BTS1} + Ag + 2H]^+$ at m/z 780.008 were found, which agreed with the 2:1 complex of **BTS1-Ag** (Fig. 5f). Based on the above investigations, the accurate structure of complex **BTS1-Ag** was proposed as insert picture in Fig. 5e.

To explore the suitable pH for the treatment of Ag^+ ions by **BTS1**, we monitored the changes of the absorption spectra over pH values ranging from 3 to13. As shown in Fig. 6a and Figure S3, for blank **BTS1** (25 μM), no obvious changes in its absorption profile and absorption intensity at 363 nm were observed in the pH range of 3–11. When pH value was above 12, its absorption intensity was decreased and a new band at 445 nm appeared, probably due to the deprotonation of

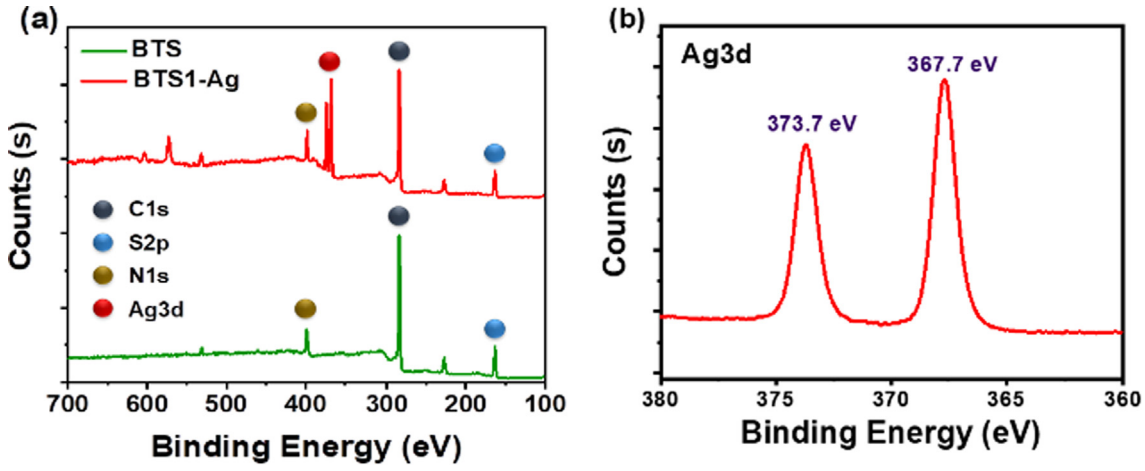

Fig. 4 (a) Wide-scan XPS spectra of **BTS1** and **BTS1-Ag**. (b) High-resolution XPS spectra of Ag3d in **BTS1-Ag**.

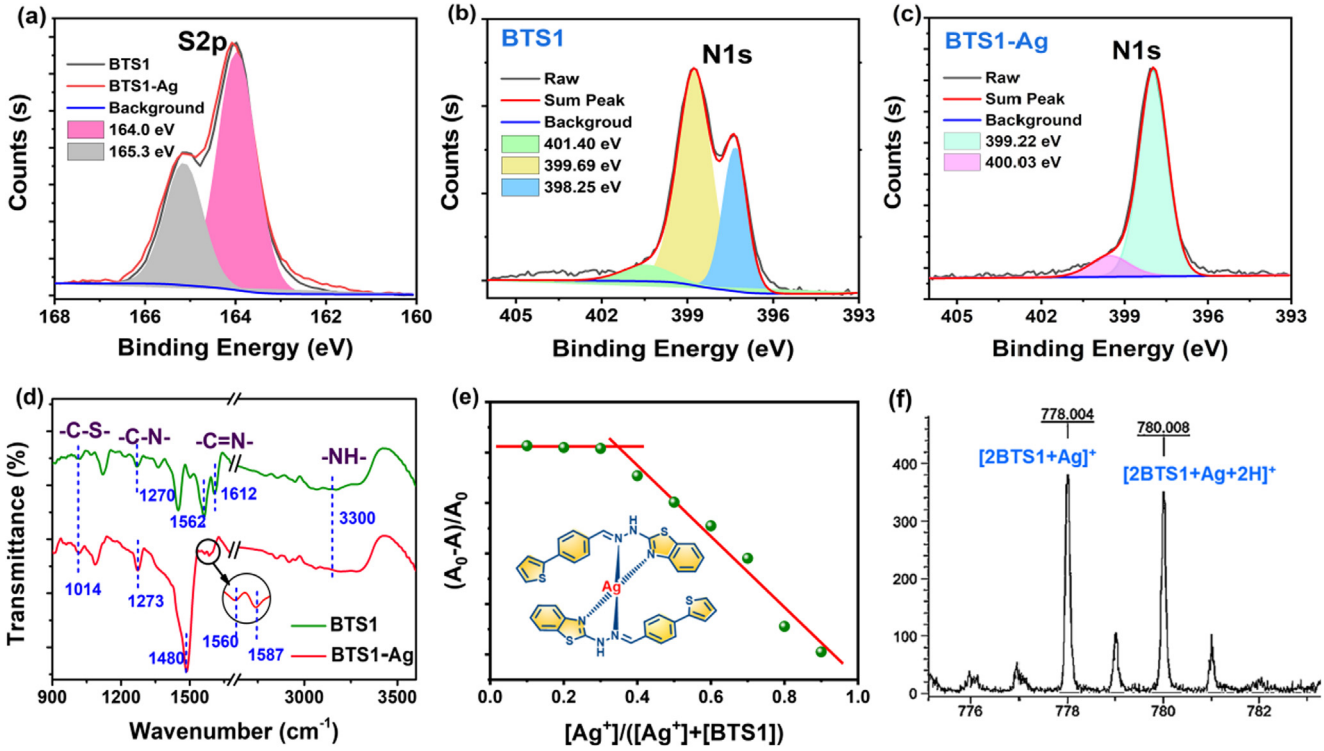

Fig. 5 High-resolution XPS spectra of (a) S2p region in **BTS1** and **BTS1-Ag**, (b) N1s region in **BTS1**, and (c) N1s region in **BTS1-Ag**. (d) FT-IR spectra of **BTS1** and **BTS1-Ag**. (e) Job's plot of **BTS1** towards Ag^+ ions (Insert: Molecular structure of **BTS1-Ag**). (f) The MS spectrum of **BTS1-Ag**.

BTS1 in the strong alkaline condition. Once a massive overdose of Ag^+ ions (10 mM) was added, the intensity of absorption was dropped obviously accompanied by precipitate formation in the pH range of 6 to 11 (Fig. 6a). The absorption profile remained constant when pH value was below 6, which can be attributed to the competitive protonation effect in acidic condition with the Ag^+ complexation. These results suggested that the optimum pH range for Ag^+ ion precipitation was 6 to 11. Consequently, the following tests were operated by using HEPES buffer (10 mM) at a neutral pH of 7.4. Additionally, the precipitation efficiency exhibited a positive correlation with both **BTS1** concentration and temperature. Precipitation rate (Q) calculated by Equation S1 as a function of temperature was plotted in Fig. 6b. When the initial concentration of **BTS1** was raised to 50 μM, the Q value reached as high as 95.4% at 50 °C.

The sensitivity of **BTS1** towards Ag^+ ions was further studied through a series of titration experiments at the pH value of 7.4 and the temperature of 25 °C. As shown in Fig. 6c, the absorption intensity at 363 nm was decreased with the increasing amount of Ag^+ ions until 0.5 equiv. of Ag^+ ions were added, which supported the 2:1 complex stoichiometry. The

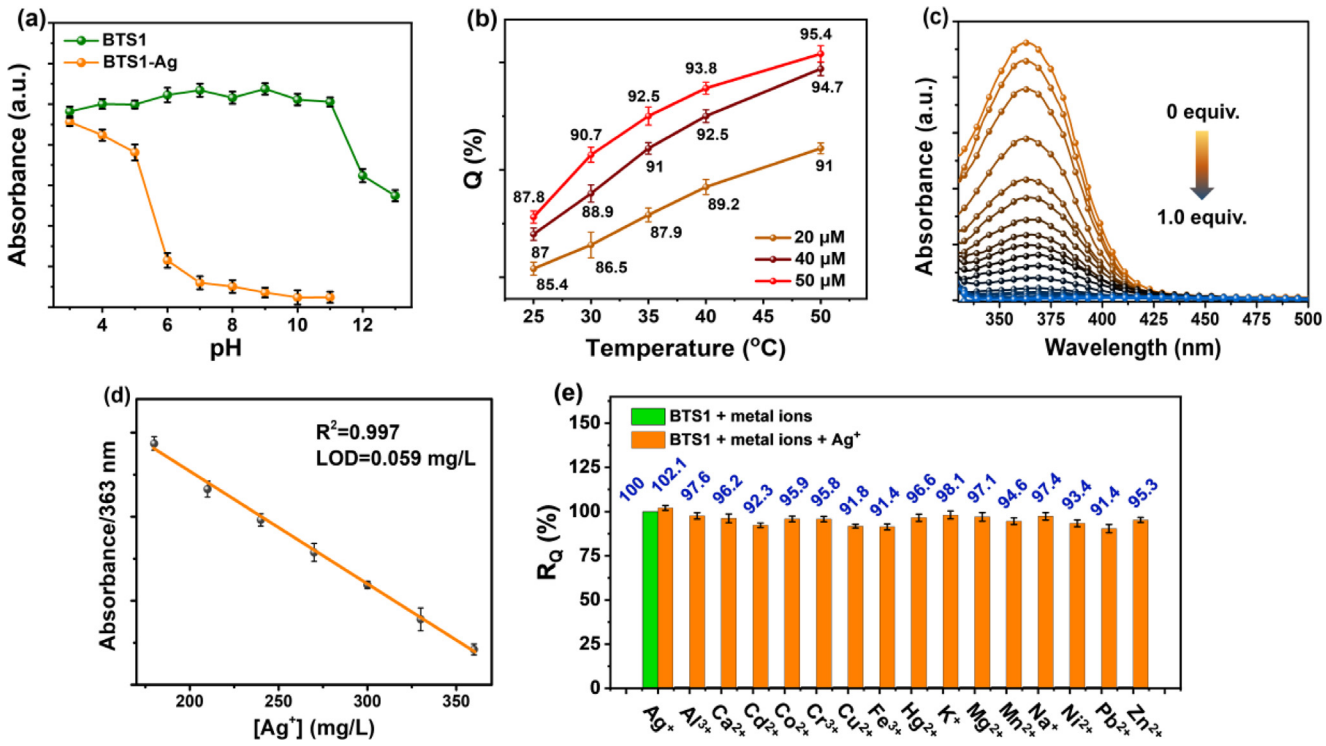

Fig. 6 (a) The absorbance changes of absorption peak at 363 nm for **BTS1** (25 μM) and **BTS1-Ag** (adding 10 mM of Ag^+ ions) under different pH conditions. (b) Q variations at different temperatures (25–50 °C) with predetermined **BTS1** concentrations (20 μM, 40 μM, 50 μM). (c) UV–vis absorption spectra of **BTS1** (25 μM) with various Ag^+ concentrations (0–1.0 equiv.). (d) The linear relationship at the concentrations of 180–360 mg/L. (e) R_Q variations in the simulated wastewater with different competing ions. Except (a), the rest were all conducted in acetone/H_2O (v/v, 1/99) HEPES buffer (10 mM, pH 7.4).

plot in Fig. 6d displayed a linear relationship between the absorption intensity at 363 nm and the Ag^+ ion concentration ranging from 180 to 360 mg/L with a linear correlation $R^2 = 0.997$. The corresponding limit of detection (LOD) of **BTS1** toward Ag^+ ions was estimated to be 0.059 mg/L, (Haldar and Lee, 2019) which was much lower than the specified value (0.5 mg/L) in *integrated wastewater discharge standard* (GB8978-1996). This result indicates that **BTS1** is highly sensitive towards Ag^+ ions. Furthermore, it is crucial for the precipitant to selectively precipitate the specific target from wastewater in the presence of potential competing species. As shown in Fig. 6e, **BTS1** exhibited high precipitation-efficiency towards Ag^+ ions in the simulated Ag^+-rich wastewater, in which the concentration of the competing metal ions was identical to that of Ag^+ ions (100 mg/L). The mass ratio (R_Q) between the silver-precipitation with and without competing ions was always within the range of 91.4%–98.1% owing to the high affinity of **BTS1** to Ag^+ ions, despite the existence of the potent competitors Pb^{2+}, Fe^{3+} and Cd^{2+}. The mass loss of precipitation in the presence of other metal ions can be attributed to the formation of soluble complexes between them and **BTS1**. Considering the obvious merits of fast chemical precipitation and high selectivity, **BTS1** should be an outstanding candidate for Ag^+ ions recovery from wastewater.

Encouraged by the superior antimicrobial property of silver complexes, we evaluated the antimicrobial activity of **BTS1-Ag** against *S. aureus* (gram-positive), and *E. coli*, *P. aeruginosa* (gram-negative) by using disc diffusion methods. The perceptivity of the bacterial strains can be confirmed from the diameter of the inhibition zone (DIZ). As depicted in Fig. 7a, clear inhibition zones can be observed around the **BTS1-Ag**-based tested papers, while almost no inhibition zone appeared around **BTS1**-based and blank test papers, indicating that **BTS1-Ag** was antimicrobial active for all tested bacterial stains. Under **BTS1-Ag** stress, *E. coli* showed a higher antibacterial sensitivity compared with other bacteria. DIZ values were 9.9 ± 0.72, 13.7 ± 0.80 and 10.3 ± 0.68 mm for *S. aureus*, *E. coli*, and *P. aeruginosa*, respectively (Fig. 7b and Table S4). We further tested the antibacterial effect of **BTS1-Ag** by varying its coating concentrations (0–4.0 g/m^2) on the test papers. As shown in Fig. 7c and 7d, the DIZ values of all bacteria strains were increased dramatically with increasing the concentration of **BTS1-Ag** in the range of 0 to 1.0 g/m^2. It was worth noting that **BTS1-Ag** still showed a certain antibacterial effect even at a low concentration of 0.25 g/m^2 with DIZ values of 8.7 ± 0.42, 9.1 ± 0.38, 9.5 ± 0.47 mm for *S. aureus*, *E. coli*, and *P. aeruginosa*, respectively. The antibacterial activity of **BTS1-Ag** maybe due to its high lipophilicity, which is beneficial to enhance the permeation of the complexes into lipid membranes and the metal binding sites prevent the enzyme activity of the microorganism. (Gönal et al., 2012) Besides, as a by-product in the recovery process, complex **BTS1-Ag** exhibited superior cost effectiveness in antibacterial field. In this way, **BTS1-Ag** with admirable antimicrobial activity supported the reutilizing strategy for silver ions from wastes into antibacterial materials.

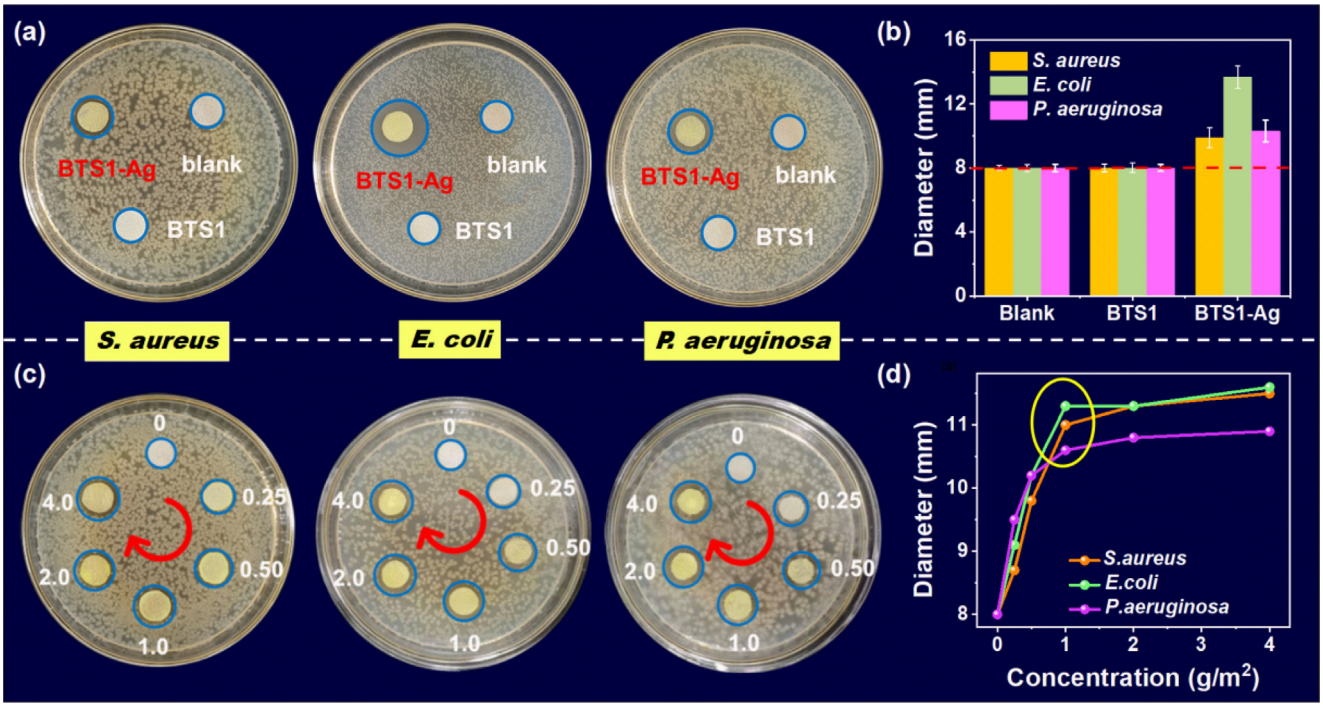

Fig. 7 (a) Antibacterial activity and (b) corresponding DIZ (mm) of blank, **BTS1** (1.0 g/m^2), and **BTS1-Ag** (1.0 g/m^2) against *S. aureus*, *E. coli* and *P. aeruginosa* in culture at 37 °C. (c) Antibacterial activity and (d) corresponding DIZ (mm) of **BTS1-Ag** with different concentrations against *S. aureus*, *E. coli* and *P. aeruginosa*.

3. Conclusions

In summary, we have shown the design and preparation of a benzothiazole Schiff base derivate **BTS1** for one-step converting Ag^+ ions from wastewater into antibacterial material through a selective chemical precipitation process. The lone pair electrons on the nitrogen atoms of imine and thiazole group provided suitable binding sites for Ag^+ ion coordination, and the planar configuration of **BTS1** further facilitated the precipitation of the complex. These combined advantages enabled **BTS1** exhibited outstanding selective precipitation with Ag^+ ions from wastewater, realizing a high precipitation rate of 95.4% towards Ag^+ ions at 50 °C. Even in the simulated wastewater containing potential competing metal ions, **BTS1** still exhibited super specific precipitation efficiency for Ag^+ ions over 98%. Most importantly, the precipitate **BTS1-Ag** can be used as antibacterial material directly, which exhibited good antibacterial activity towards *S. aureus*, *E. coli* and *P. aeruginosa*. In consideration of **BTS1** with high selectivity and precipitation rate towards Ag^+ ions, as well as the good antibacterial activity of **BTS1-Ag**, the precipitant **BTS1** developed in this study is a promising precipitant for practical recovery and reutilization of Ag^+ ions from wastewater by one-step.

Declaration of Competing Interest

The authors declare that they have no known competing financial interests or personal relationships that could have appeared to influence the work reported in this paper.

Acknowledgements

The work was supported by the National Natural Science Foundation of China (61605138), Shanxi Scholarship Council of China (No. 2021-057) and the Natural Science Foundation of Shanxi Province (No. 20210302123144).

Appendix A. Supplementary material

Supplementary data to this article can be found online at https://doi.org/10.1016/j.arabjc.2023.104836.

References

Abbas, A.A., Abdellattif, M.H., Dawood, K.M., 2022. Inhibitory activities of bipyrazoles: a patent review. Expert Opin Ther Pat 32 (1), 63–87.

Adeleke, A.A., Zamisa, S.J., Islam, M.S., Olofinsan, K., Salau, V.F., Mocktar, C., Omondi, B., 2021. Quinoline functionalized Schiff Base Silver (I) complexes: interactions with biomolecules and in vitro cytotoxicity, antioxidant and antimicrobial activities. Molecules 26 (5), 1205.

Ahmad, F., Ashraf, N., Zhou, R.-B., Chen, J.J., Liu, Y.-L., Zeng, X., Zhao, F.-Z., Yin, D.-C., 2019. Optimization for silver remediation from aqueous solution by novel bacterial isolates using response surface methodology: recovery and characterization of biogenic AgNPs. J. Hazard. Mater. 380, 120906.

Akcil, A., Erust, C., Gahan, C.S., Ozgun, M., Sahin, M., Tuncuk, A., 2015. Precious metal recovery from waste printed circuit boards using cyanide and non-cyanide lixiviants–a review. Waste Manage. 45, 258–271.

Allawadhi, P., Singh, V., Khurana, A., Khurana, I., Allwadhi, S., Kumar, P., Banothu, A.K., Thalugula, S., Barani, P.J., Naik, R.R., Bharani, K.K., 2021. Silver nanoparticle based multifunctional approach for combating COVID-19. Sens. Int. 2, 100101.

Bas, A.D., Yazici, E.Y., Deveci, H., 2012. Recovery of silver from X-ray film processing effluents by hydrogen peroxide treatment. Hydrometallurgy 121–124, 22–27.

Chen, Q., Yao, Y., Li, X., Lu, J., Zhou, J., Huang, Z., 2018. Comparison of heavy metal removals from aqueous solutions by

chemical precipitation and characteristics of precipitates. J. Water Process. Eng. 26, 289–300.
Chernousova, S., Epple, M., 2013. Silver as antibacterial agent: ion, nanoparticle, and metal. Angew. Chem. Int. Ed. 52 (6), 1636–1653.
Fu, F., Chen, R., Xiong, Y., 2007. Comparative investigation of N, N'-bis-(dithiocarboxy) piperazine and diethyldithiocarbamate as precipitants for Ni(II) in simulated wastewater. J. Hazard. Mater. 142 (1–2), 437–442.
Gönal, S., Kaloğlu, N., İzdemir, S., Demir, İ.Ö., 2012. Novel benzimidazolium salts and their silver complexes: Synthesis and antibacterial properties. Inorg. Chem. Commun. 2, 142–146.
Haldar, U., Lee, H.I., 2019. BODIPY-derived polymeric chemosensor appended with thiosemicarbazone units for the simultaneous detection and separation of Hg(II) ions in pure aqueous media. ACS Appl. Mater. Interfaces 11 (14), 13685–13693.
Hamouda, T., Ibrahim, H.M., Kafafy, H.H., Mashaly, H.M., Mohamed, N.H., Aly, N.M., 2021. Preparation of cellulose-based wipes treated with antimicrobial and antiviral silver nanoparticles as novel effective high-performance coronavirus fighter. Int. J. Biol. Macromol 181, 990–1002.
Ho, N.A.D., Babel, S., 2021. Bioelectrochemical technology for recovery of silver from contaminated aqueous solution: a review. Environ. Sci. Pollut. Res. 28 (45), 63480–63494.
Ibrahim, N., Akindoyo, J.O., Mariatti, M., 2022. Recent development in silver-based ink for flexible electronics. J. Sci-Adv. Mater. Dev. 7, (1) 100395.
Khan, S., Chen, X., Almahri, A., Allehyani, E.S., Alhumaydhi, F.A., Ibrahim, M.M., Ali, S., 2021. Recent developments in fluorescent and colorimetric chemosensors based on Schiff bases for metallic cations detection: a review. J. Environ. Chem. Eng. 9, (6) 106381.
Law, S., Lo, C., Han, J., Leung, A.W., Xu, C., 2022. Could curcumin modified silver nanoparticles treat COVID-19. Adv. Pharm. Bull. 12 (1), 5–6.
Li, P., Jiang, H., Barr, A., Ren, Z., Gao, R., Wang, H., Fan, W., Zhu, M., Xu, G., Li, J., 2021. Reusable polyacrylonitrile-sulfur extractor of heavy metal ions from wastewater. Adv. Funct. Mater. 31 (51), 2105845.
Ling, L., Huang, X.Y., Zhang, W.X., 2018. Enrichment of precious metals from wastewater with core-shell nanoparticles of iron. Adv. Mater. 30 (17), e1705703.
S.P. Mary Jenisha Barnabas, Saravanan Nagappan, Ildoo Chung and Chang-Sik Ha, Silver (I)- Schiff-base complex intercalated layered double hydroxide with antimicrobial activity, Adv. Nano. Res. 4 (2021) 473
Morozova, O.V., Manuvera, V.A., Grishchechkin, A.E., Barinov, N. A., Shevlyagina, N.V., Zhukhovitsky, V.G., Lazarev, V.N., Klinov, D.V., 2022. Targeting of silver cations, silver-cystine complexes, Ag nanoclusters, and nanoparticles towards SARS-CoV-2 RNA and recombinant virion proteins. Viruses 14 (5), 902.
Qian, H.L., Meng, F.L., Yang, C.X., Yan, X.P., 2020. Irreversible amide-linked covalent organic framework for selective and ultrafast gold recovery. Angew. Chem. Int. Ed. 59 (40), 17607–17613.
Quiton, K.G.N., Huang, Y.-H., Lu, M.-C., 2022. Recovery of cobalt and copper from single- and co-contaminated simulated electroplating wastewater via carbonate and hydroxide precipitation. Sustain. Environ. Res. 32 (1), 31.
Ratte, H.T., 1999. Bioaccumulation and toxicity of silver compounds: a review. Environ. Toxicol. Chem. 18 (1), 89–108.
Sverdrup, H., Koca, D., Ragnarsdottir, K.V., 2014. Investigating the sustainability of the global silver supply, reserves, stocks in society and market price using different approaches. Resour. Conserv. Recycl. 83, 121–140.
Teirumnieks, E., Balchev, I., Ghalot, R.S., Lazov, L., 2020. Antibacterial and anti-viral effects of silver nanoparticles in medicine against COVID-19—a review. Laser Phys 31, (1) 013001.
Wang, L., Deng, M., Xu, H., Li, W., Huang, W., Yan, N., Zhou, Y., Chen, J., Qu, Z., 2020. Selective reductive removal of silver ions from acidic solutions by redox-active covalent organic frameworks. ACS Appl. Mater. Interfaces 12 (33), 37619–37627.
Wang, H., Ren, Z.J., 2014. Bioelectrochemical metal recovery from wastewater: a review. Water Res. 66, 219–232.
Wang, L., Wang, K., Huang, R., Qin, Z., Su, Y., Tong, S., 2020. Hierarchically flower-like WS2 microcrystals for capture and recovery of Au (III), Ag (I) and Pd (II). Chemosphere 252, 126578.
Wang, X., Wang, L., Ma, S., Tong, S., 2023. Ultrathin WS2 nanobowls-based hybrid aerogels for selective trapping of precious metals from electronic wastes and elimination of organic dyes. Chem. Eng. J. 451, 138539.
Wen, Q., Di, J., Zhao, Y., Wang, Y., Jiang, L., Yu, J., 2013. Flexible inorganic nanofibrous membranes with hierarchical porosity for efficient water purification. Chem. Sci. 4 (12).
Xie, J., Zhong, Y., Yu, Y., Wang, M., Guo, Z., 2022. Green capturing of Ag from ultra-low concentration precious metal wastewater by electrodeposition assisted with electrocoagulation: electrochemical behavior and floc characterization. Process Saf Environ Prot 167, 592–600.
Xu, J., Cao, Z., Zhang, Y., Yuan, Z., Lou, Z., Xu, X., Wang, X., 2018. A review of functionalized carbon nanotubes and graphene for heavy metal adsorption from water: Preparation, application, and mechanism. Chemosphere 195, 351–364.
Xue, W., Huang, D., Wen, X., Chen, S., Cheng, M., Deng, R., Li, B., Yang, Y., Liu, X., 2020. Silver-based semiconductor Z-scheme photocatalytic systems for environmental purification. J. Hazard. Mater. 390, 122128.
Yan, F., Sun, J., Zang, Y., Sun, Z., Zhang, H., Wang, X., 2020. Benzothiazole applications as fluorescent probes for analyte detection. J. Iran. Chem. Soc. 17 (12), 3179–3203.
Yang, F., Yan, Z., Zhao, J., Miao, S., Wang, D., Yang, P., 2020. Rapid capture of trace precious metals by amyloid-like protein membrane with high adsorption capacity and selectivity. J. Mater. Chem. A 8 (6), 3438–3449.
Yazici, E.Y., Yilmaz, E., Ahlatci, F., Celep, O., Deveci, H., 2017. Recovery of silver from cyanide leach solutions by precipitation using Trimercapto- s -triazine (TMT). Hydrometallurgy 174, 175–183.
Ying, X., Fang, Z., 2006. Experimental research on heavy metal wastewater treatment with dipropyl dithiophosphate. J. Hazard. Mater. 137 (3), 1636–1642.
Zeng, S., Li, S.J., Sun, X.J., Li, M.Q., Xing, Z.Y., Li, J.L., 2019. A benzothiazole-based chemosensor for significant fluorescent turn-on and ratiometric detection of Al3 + and its application in cell imaging. Inorg. Chim. Acta 486, 654–662.
Zhao, X., Li, X., Wang, Y., Lin, J., Liu, J., Shao, H., 2020. Degradation of organics with simultaneous recovery of silver in a simple visible-light responsive dual photoelectrode photocatalytic fuel cell. Environ. Sci.: Water Res. Technol. 6 (7), 1869–1879.